

Modeling the Conductor Losses of Thick Multiconductor Coplanar Waveguides and Striplines: A Conformal Mapping Approach

*Original*

Modeling the Conductor Losses of Thick Multiconductor Coplanar Waveguides and Striplines: A Conformal Mapping Approach / Bertazzi, Francesco; Camarchia, Vittorio; Goano, Michele; Pirola, Marco; Ghione, Giovanni. - In: IEEE TRANSACTIONS ON MICROWAVE THEORY AND TECHNIQUES. - ISSN 0018-9480. - STAMPA. - 64:4(2016), pp. 1217-1227. [10.1109/TMTT.2016.2535395]

*Availability:*

This version is available at: 11583/2638910 since: 2016-04-02T14:28:05Z

*Publisher:*

IEEE

*Published*

DOI:10.1109/TMTT.2016.2535395

*Terms of use:*

This article is made available under terms and conditions as specified in the corresponding bibliographic description in the repository

*Publisher copyright*

(Article begins on next page)

# Modelling the conductor losses of thick multiconductor coplanar waveguides and striplines: a conformal mapping approach

Francesco Bertazzi, Vittorio Camarchia *Senior Member, IEEE*, Michele Goano *Member, IEEE*,  
Marco Pirola *Member, IEEE* and Giovanni Ghione *Fellow, IEEE*

**Abstract**—A conformal mapping approach to model the skin-effect conductor losses of thick multiconductor coplanar waveguides and multiconductor coplanar strips is proposed. The model allows for arbitrary strip or slot number and widths and is accurate for conductor thicknesses up to around 40% of the minimum strip and slot width. Examples are presented to demonstrate the accuracy of the approach when compared to the results from a FEM numerical code.

**Index Terms**—Conformal mapping, coplanar lines, finite-element method, skin effect losses, Schwarz-Christoffel mapping

## I. INTRODUCTION

MULTICONDUCTOR coplanar lines (MCLs), i.e., multiconductor coplanar waveguides (MCPWs) and multiconductor coplanar strips (MCPSs), see Fig. 1, are building blocks in analog and digital circuits [1], [2]. Relevant examples are interdigitated MCPW couplers in coplanar Microwave Monolithic Integrated Circuits (MMICs) [3] and high-speed MCPS interconnects [4]. The analysis of MCL conductor

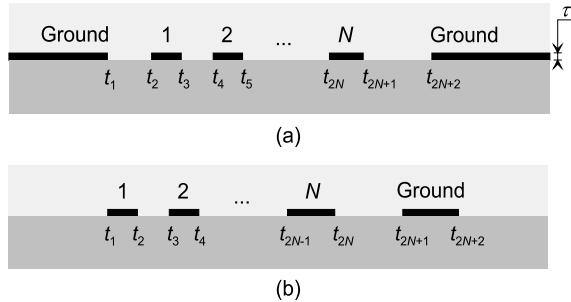


Fig. 1. Multiconductor coplanar lines (MCLs): (a) Multiconductor coplanar waveguide, MCPW; (b) Multiconductor coplanar strips, MCPS. The strip thickness is  $\tau$  and the parameters  $t_i$ ,  $i = 1 \dots 2N + 2$ , define the line geometry.

losses can be carried out at an arbitrary frequency through full-wave and quasi-static electromagnetic (EM) approaches based on differential formulations, like the Finite Element

Method (FEM) [5], [6]. The entire domain, including the conductors' interior, must be discretized and the analysis of open structures requires large computational boxes to avoid artifacts from boundary conditions. In the high-frequency, skin-effect regime, conductor losses can be approximated by integrating the square of the surface longitudinal current density  $J_z$ , and taking advantage of the surface impedance concept [7, (26)]. A perturbative approach is often adopted, evaluating  $J_z$  in the presence of perfect conductors. The surface current density can be in turn computed through the moment method (MoM) solution of the quasi-static [7], [8] or full wave integral formulation of the EM problem [9], [10].

While numerical techniques offer the greatest flexibility in terms of line geometry and materials, they may become too CPU intensive or inaccurate when the number of strips is large or with extreme form factors, as in low-crosstalk MCPSs, see the geometry in [4, Sec. 3.5.4]. In FEM solvers not adopting impedance boundary conditions [11] the design of a properly dense mesh also becomes critical when  $\tau \gg \delta$ , where  $\delta$  is the skin penetration depth. Moreover, such techniques often are too computationally expensive to be easily used in inverse or optimization problems.

Conformal mapping (CM) is a computationally efficient tool to evaluate the longitudinal current density of MCLs, that can be approximated, in the presence of ideal conductors, by the static surface charge distribution [12]. An early example of the CM loss evaluation for a rectangular conductor, together with a discussion of the accuracy of the surface resistance approach when conductors with sharp rectangular edges are considered, is presented in [13]. On the basis of the CM approximation of the surface current density, closed-form expressions have been presented for the losses of coplanar waveguides (CPW) and striplines (CPS) [14], [15], [16], [17] and of symmetrical CPW couplers [18]. Expressions for the CPW attenuation were also presented in [19, Sec. 7.4.2], based on Wheeler's incremental inductance rule [20], and in [21], where a stopping-distance formulation is adopted that leads, in the high-frequency limit, to the result in [14].

The loss analysis of MCLs with  $N$  conductors plus a ground plane, where  $N > 1$  and no symmetries exist that allow for even and odd mode excitations [18], requires to introduce a set of  $N$  linearly independent mappings, corresponding to suitable line excitations. This technique, first proposed in [22] for the evaluation of the capacitance matrix of zero-thickness multiconductor striplines, was extended in [23] to the case of

Manuscript submitted on 13/10/2015, revised on 26/01/2016, accepted on 16/02/2016... F. Bertazzi and M. Goano are with the Dipartimento di Elettronica e Telecomunicazioni and with IEIIT-CNR, Politecnico di Torino, Corso Duca degli Abruzzi 24, 10129 Torino, Italy. V. Camarchia, M. Pirola, and G. Ghione are with the Dipartimento di Elettronica e Telecomunicazioni, Politecnico di Torino, Corso Duca degli Abruzzi 24, 10129 Torino, Italy. e-mail: vittorio.camarchia@polito.it

zero-thickness MCPWs and MCPs. For MCPWs, a suitable set of  $N$  mappings corresponds to boundary conditions where, in mapping  $i = 1 \dots N$ , the ground planes are at zero potential, strip  $i$  is at potential 1, and strips  $j \neq i$  have zero total charge. For MCPs, a suitable dual set for mapping  $i = 1 \dots N$  is given by strips  $1 \dots i$  being at potential 1, while all other strips and the rightmost ground plane are at zero potential.

In the presence of thick strips, however, an intermediate mapping is needed to transform the thick line into a zero-thickness one. Such a mapping has a dual purpose, (1) to lead to a much more accurate approximation of the capacitance matrix in the presence of thick conductors, and (2) to introduce a square-integrable representation of the surface current density. The total surface current density can be approximated as a superposition of  $N$  linearly independent excitations associated to the  $N$  mappings; this enables to directly express, through the surface resistance  $R_s$ , the dissipated power density, and to estimate the per-unit-length (*p.u.l.*) resistance matrix by integrating it on the line and ground plane peripheries. A partial preliminary report on MCL skin-effect losses was presented in [24].

The analytical approximations discussed are consistent with the results in [14], [15], [16] in the thin strip limit, but the present formulation not only applies to an arbitrary number of conductors, but provides a more accurate estimate of the *p.u.l.* resistance, inductance and capacitance (matrices) for thick lines. The examples shown suggest that the technique is accurate even for a strip thickness as large as 40% of the minimum slot and strip width.

The paper is organized as follows: Sec. II reports a summary of the conformal mapping procedure for the lossless case, extending the treatment to finite-thickness lines. Sec. III is devoted to the loss analysis, whose results are reported in Sec. III-A and Sec. III-B for the MCPW and MCPs, respectively. Sec. IV briefly introduces the characteristic modal parameters for a MCL supported by a semi-infinite dielectric substrate. Analytical details on the thick-to-thin strip transformation are reported in Appendix A. Sec. V is devoted to some numerical examples, while conclusions are drawn in Sec. VI.

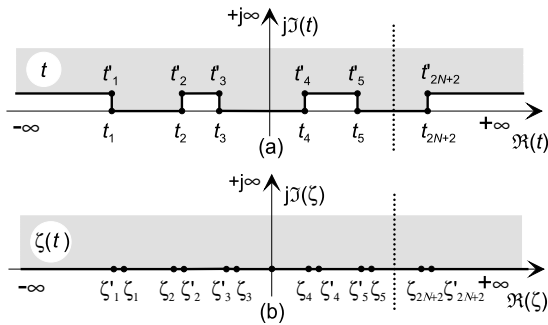


Fig. 2. Thick-to-thin mapping for the MCPW (upper half space): (a)  $t$ -plane; (b) transformed  $\zeta$  plane.

## II. CONFORMAL MAPPING ANALYSIS

Let us summarize the CM procedure introduced in [23] focusing the analysis of the line *in vacuo*, which is the

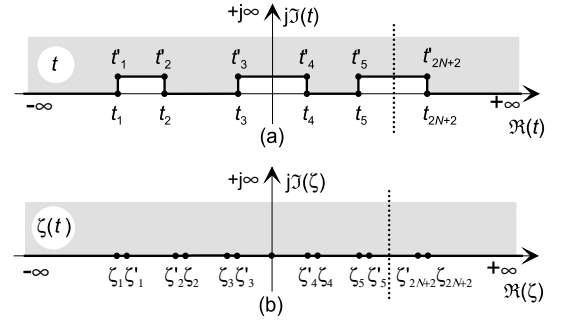


Fig. 3. Thick-to-thin mapping for the MCPs (upper half space): (a)  $t$ -plane; (b) transformed  $\zeta$  plane.

basis for the evaluation of the *p.u.l.* resistance matrix of the MCL. As already recalled, the high-frequency current density distribution of the line corresponds to the static charge distribution. Since this distribution is not square-integrable in a line with infinitely thin conductors, we extend, as a first step, the analysis of zero-thickness MCLs [23] to lines with conductors having finite thickness  $\tau$ .

To this aim, an additional Schwarz-Christoffel (SC) mapping is introduced. The mapping, defined in (1), transforms the upper half of the finite thickness structure ( $t$ -plane, line half thickness  $|t'_i - t_i| = \tau/2$ ) into the upper half of the zero-thickness structure ( $\zeta$ -plane), see Fig. 2 and Fig. 3 for the MCPW and MCPs case, respectively. For both lines the mapping reads:

$$\frac{dt}{d\zeta} = \prod_{i=1}^{2N+2} \sqrt{\frac{\zeta'_i - \zeta}{\zeta_i - \zeta}}. \quad (1)$$

If  $\tau$  is suitably smaller than the strip and slot widths, (1) can be approximately integrated on the strip lateral sides, strip tops and slots (see Appendix A). This enables to define the strip and slot coordinates in the  $\zeta$  plane in terms of strip and slot width corrections. Physically, the extra capacitance introduced by the thick strips translates into an increase of the strip widths and decrease of the slot widths in the transformed zero-thickness structure having the same capacitance.

Consider first a MCPW with  $N$  strips; the coordinate index in the  $t$  and  $\zeta$  planes goes from 1 to  $2N + 2$ . The  $t$ -plane coordinates are defined in terms of the strip widths  $w_i^{\text{MCPW}}$  ( $i = 1 \dots N$ ) and the slot widths  $s_i^{\text{MCPW}}$  ( $i = 1 \dots N + 1$ ) as:

$$t'_{2i+1} - t'_{2i} = w_i^{\text{MCPW}}, \quad i = 1 \dots N, \quad (2)$$

$$t_{2i} - t_{2i-1} = s_i^{\text{MCPW}}, \quad i = 1 \dots N + 1 \quad (3)$$

$$t'_{2i} - t_{2i} = t'_{2i-1} - t_{2i-1} = j\frac{\tau}{2} \quad i = 1 \dots N + 1. \quad (4)$$

The  $\zeta$  plane coordinates can be now recovered adopting the strip side length and width corrections reported in (14), (15), respectively, and the slot width correction in (16):

$$\zeta'_{2i+1} - \zeta'_{2i} = w_i^{\text{MCPW}} + \Delta w_i^{\text{MCPW}}, \quad i = 1 \dots N, \quad (5)$$

$$\zeta_{2i} - \zeta_{2i-1} = s_i^{\text{MCPW}} - \Delta s_i^{\text{MCPW}}, \quad i = 1 \dots N + 1 \quad (6)$$

$$\zeta'_{2i} - \zeta_{2i} \approx \zeta_{2i-1} - \zeta'_{2i-1} \approx \Delta\zeta \quad i = 1 \dots N + 1, \quad (7)$$

where the strip side correction  $\Delta\zeta$  results to be approximately independent on the strip index.

Similarly, for a MCPS with  $N$  strips and a lateral ground plane (strip  $N + 1$ ) the  $t$  plane coordinates read:

$$t'_{2i} - t'_{2i-1} = w_i^{\text{MCPS}}, \quad i = 1 \dots N + 1, \quad (8)$$

$$t_{2i+1} - t_{2i} = s_i^{\text{MCPS}}, \quad i = 1 \dots N, \quad (9)$$

$$t'_{2i} - t_{2i} = t'_{2i-1} - t_{2i-1} = j \frac{\tau}{2} \quad i = 1 \dots N + 1, \quad (10)$$

while for the  $\zeta$  plane coordinates we have:

$$\zeta'_{2i} - \zeta'_{2i-1} = w_i^{\text{MCPS}} + \Delta w_i^{\text{MCPS}}, \quad i = 1 \dots N + 1 \quad (11)$$

$$\zeta_{2i-1} - \zeta_{2i} = s_i^{\text{MCPS}} - \Delta s_i^{\text{MCPS}}, \quad i = 1 \dots N \quad (12)$$

$$\zeta'_{2i-1} - \zeta_{2i-1} = \zeta_{2i} - \zeta'_{2i} \approx \Delta \zeta \quad i = 1 \dots N + 1 \quad (13)$$

where the MCPS strip side length and width corrections are reported in (14), (17), respectively, and the slot width correction is in (18).

Expressions for the parameters  $\Delta \zeta$ ,  $\Delta w_i$  and  $\Delta s_i$  are discussed in Appendix A; the expressions for  $\Delta w_i$  and  $\Delta s_i$  are novel and more accurate than those previously available in the literature, cfr. [14, p. 51, (18) and (19)] and [19, Sec. 7.3.3]). We have for both the MCPW and the MCPS, independent of the strip (or ground) side considered:

$$\Delta \zeta \approx \frac{\tau}{\pi} \quad (14)$$

see (61) and (62) in Appendix A. Following the discussion presented in Appendix A, the MCPW strip and slot corrections read:

$$\Delta w_i^{\text{MCPW}} = \Delta \zeta \left( \log \frac{4w_i^{\text{MCPW}}}{\Delta \zeta} - 1 \right) - \frac{\Delta \zeta w_i^{\text{MCPW}}}{2} \times \left( \sum_{j=1}^{2i-1} \frac{(-1)^{j+1}}{\langle t \rangle_{\text{Strip } i} - t_j} + \sum_{j=2i+2}^{2N+2} \frac{(-1)^j}{t_j - \langle t \rangle_{\text{Strip } i}} \right) \quad (15)$$

$$\Delta s_i^{\text{MCPW}} = \Delta \zeta \left( \log \frac{4s_i^{\text{MCPW}}}{\Delta \zeta} + 1 \right) + \frac{\Delta \zeta s_i^{\text{MCPW}}}{2} \times \left( \sum_{j=1}^{2i-2} \frac{(-1)^{j+1}}{\langle t \rangle_{\text{Slot } i} - t_j} + \sum_{j=2i+1}^{2N+2} \frac{(-1)^j}{t_j - \langle t \rangle_{\text{Slot } i}} \right) \quad (16)$$

$$\langle t \rangle_{\text{Strip } i}^{\text{MCPW}} = \frac{t_{2i+1} + t_{2i}}{2}, \quad \langle t \rangle_{\text{Slot } i}^{\text{MCPW}} = \frac{t_{2i} + t_{2i-1}}{2}.$$

For the MCPS we similarly have:

$$\Delta w_i^{\text{MCPS}} = \Delta \zeta \left( \log \frac{4w_i^{\text{MCPS}}}{\Delta \zeta} - 1 \right) + \frac{\Delta \zeta w_i^{\text{MCPS}}}{2} \times \left( \sum_{j=1}^{2i-2} \frac{(-1)^j}{\langle t \rangle_{\text{Strip } i}^{\text{MCPS}} - t_j} + \sum_{i=2i+1}^{2N+2} \frac{(-1)^{j+1}}{t_j - \langle t \rangle_{\text{Strip } i}^{\text{MCPS}}} \right) \quad (17)$$

$$\Delta s_i^{\text{MCPS}} = \left( \log \frac{4s_i^{\text{MCPS}}}{\Delta \zeta} + 1 \right) \Delta \zeta + \frac{\Delta \zeta s_i^{\text{MCPS}}}{2} \times \left( \sum_{j=1}^{2i-1} \frac{(-1)^j}{\langle t \rangle_{\text{Slot } i}^{\text{MCPS}} - t_j} + \sum_{i=2i+2}^{2N+2} \frac{(-1)^{j+1}}{t_j - \langle t \rangle_{\text{Slot } i}^{\text{MCPS}}} \right) \quad (18)$$

$$\langle t \rangle_{\text{Strip } i}^{\text{MCPS}} = \frac{t_{2i} + t_{2i-1}}{2}, \quad \langle t \rangle_{\text{Slot } i}^{\text{MCPS}} = \frac{t_{2i+1} + t_{2i}}{2}.$$

Using (14) - (18) the finite-thickness MCPW or MCPS can be mapped on the corresponding zero-thickness structures in the  $\zeta$  plane.

From the zero-thickness structure we evaluate the line parameters following [23, Sec. 2.1 and 2.2]. Since a system with  $N$  strips plus ground plane supports  $N$  independent excitations, the analysis of the *p.u.l.* capacitance matrix *in vacuo*  $\mathbf{C}_0 = 2\mathbf{C}_{\text{uh}0}$ , where  $\mathbf{C}_{\text{uh}0}$  is the capacitance matrix of the upper half of the line, requires a system of  $N$  SC mappings, see [23, Sec. 2.1 and 2.2]. In the next subsections we will summarize the CM procedure for MCPWs (Sec. II-A) and MCPSs (Sec. II-B) following the matrix notation of [23] and only reporting results relevant to loss analysis.

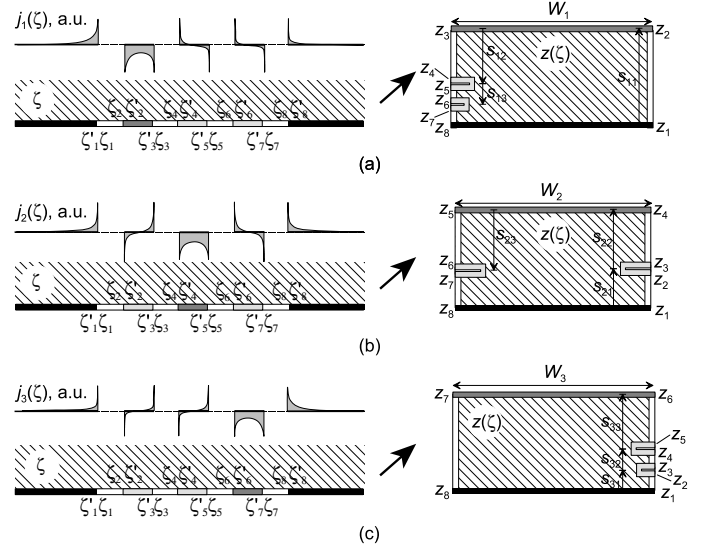


Fig. 4. Set of SC mappings (a), (b), and (c) for a three-conductor symmetric MCPW. The ground planes are drawn as black segments, white segments are magnetic walls, the  $k$ -th conductor is dark grey while the other ones are pale grey. The right-hand side  $z$  planes are to scale, assuming  $W_k = W$ ,  $k = 1 \dots 3$ . The normalized static charge, i.e., the high-frequency surface current density distribution, is shown in the left side (above) for each mapping. All strips but one have zero total charge (current), while the charge (current) carried by the unfolded strip has opposite sign with respect to the one in the ground plane.

#### A. Multiconductor coplanar waveguide (MCPW)

To evaluate the upper half-space *in vacuo* capacitance of the MCPW,  $\mathbf{C}_{\text{uh}0}^{\text{MCPW}}$ , a set of  $N$  SC mappings is introduced transforming the upper-half  $\zeta$ -plane into the interior of a rectangle in  $z$ -plane; an example with  $N = 3$  is shown in Fig. 4. In the  $k$ -th mapping, the  $k$ -th line is on top of the rectangle, the ground plane, extending to infinity in the  $t$  and  $\zeta$ -planes, is at the bottom of the rectangle, and all remaining strips  $j \neq k$  are *folded* on the rectangle sides, parallel to the top and bottom sides. Defining  $D(\zeta) = \prod_{i=1}^{2N+2} \sqrt{\zeta - \zeta_i}$ , the  $k$ -th mapping reads:

$$\frac{dz_k}{d\zeta} = A_k \frac{\prod_{i=1, \neq k}^N (\zeta - \zeta_{ki})}{D(\zeta)} = \frac{1}{D(\zeta)} \sum_{i=1}^N a_{ki} \zeta^{i-1}. \quad (19)$$

The parameters  $\zeta_{k1} \dots \zeta_{kN}$  or, equivalently, the coefficients of the polynomial expansion  $a_{k1} \dots a_{kN}$  can be determined imposing that the  $k$ -th strip is *unfolded* in the  $z$ -plane while

the others are *folded* in point  $\zeta_{ki}$ ; this corresponds to the conditions:

$$\int_l \frac{dz_k}{d\zeta} d\zeta = \int_l dz_k = z_{2k+1} - z_{2k} = -W_k, \quad l = k \quad (20)$$

$$\int_l \frac{dz_k}{d\zeta} d\zeta = \int_l dz_k = z_1 - z_{2N+2} = W_k, \quad l = N + 1 \quad (21)$$

$$\int_l \frac{dz_k}{d\zeta} d\zeta = \int_l dz_k = z_{2l+1} - z_{2l} = 0, \quad l \neq k \quad (22)$$

where the integral is extended to strip  $l$ , and the rectangle width  $W_k$  can be scaled arbitrarily without affecting the value of the capacitance or resistance *p.u.l.* matrices. From (19), conditions (20) and (22) can be written as:

$$\sum_{i=1}^N a_{ki} F_{ik} = -W_k, \quad \sum_{i=1}^N a_{ki} F_{ij} = 0 \quad (j \neq k), \quad (23)$$

where:

$$F_{ij} = \int_{\zeta_{2j}}^{\zeta_{2j+1}} \frac{\zeta^{i-1}}{D(\zeta)} d\zeta. \quad (24)$$

On defining the matrices  $\mathbf{F} = [F_{ij}]$ ,  $\mathbf{a} = [a_{ij}]$ ,  $\mathbf{W} = \text{diag}\{W_k\}$ , the above set can be expressed in compact form for all mappings ( $k = 1 \dots N$ ) as  $\mathbf{a} \cdot \mathbf{F} = -\mathbf{W}$ ; therefore:

$$\mathbf{a} = -\mathbf{W} \cdot \mathbf{F}^{-1}, \quad (25)$$

which defines the coefficients of all sets of CMs. Following the procedure in [23, Sec. 2.1], we finally obtain the half-space capacitance matrix of the MCPW as:

$$\mathbf{C}_{\text{uh0}}^{\text{MCPW}} = -\epsilon_0 \mathbf{U}^{-1} \cdot \mathbf{G}^{-1} \cdot \mathbf{F}, \quad (26)$$

where the elements of  $\mathbf{U}^{-1}$  are  $U_{ij}^{-1} = \delta_{ij} - \delta_{i+1,j}$ ,  $\delta_{ij}$  is the Kronecker delta, and

$$G_{ij} = \frac{1}{\sqrt{-1}} \int_{\zeta_{2j-1}}^{\zeta_{2j}} \frac{\zeta^{i-1}}{D(\zeta)} d\zeta. \quad (27)$$

The hyperelliptic integrals in (24) and (27) can be efficiently evaluated through Gauss-Chebyshev quadrature formulae as discussed in [23, Sec. 3]. For  $N = 1$  and for  $N = 2$  (symmetrical lines only)  $F_{ij}$  and  $G_{ij}$  can be expressed in terms of complete elliptic integrals.

### B. Multiconductor coplanar strips (MCPS)

In the complementary structure (MCPS) we have  $N + 1$  strips, the last one being the ground plane, separated by  $N$  slots. To compute the *in vacuo* capacitance of the upper half of the MCPS,  $\mathbf{C}_{\text{uh0}}^{\text{MCPS}}$ , we adopt the same set of SC mappings already introduced for the MCPW. In the  $k$ -th mapping, the outer slot (extending to  $-\infty$ ) is at the bottom of the rectangle in the  $z$ -plane, the  $k$ -th one lies on top of the rectangle, and all other slots are folded. The width of the unfolded slot  $S_k$  can be chosen arbitrarily. All strips  $i \leq k$  are on the right-hand side of the rectangle, while those for  $i > k$  are on the left-hand side. A convenient boundary condition, leading to a parallel-plate geometry, is as follows: all strips mapped on the right-hand side of the rectangle in  $z$  plane ( $l \leq k$ ) have potential  $V_k$ , all strips on the left-hand side ( $l > k$ ), including the ground ( $l = N + 1$ ) are grounded. As an example,

the mappings for a three-slot MCPS are shown in Fig. 5. By imposing the folding and unfolding conditions one can again derive the polynomial coefficient matrix as  $\mathbf{a} = -\mathbf{S} \cdot \mathbf{F}^{-1}$  where  $\mathbf{S} = \text{diag}\{S_k\}$ . Integration along strips [23, p. 71, left column, around (26)] yields for the  $k$ -th mapping the strip widths  $w_{kj}$  in the transformed plane. On defining  $\mathbf{w} = [w_{kj}]$  we have:

$$\mathbf{w} = -\mathbf{S} \cdot \mathbf{F}^{-1} \cdot \mathbf{G}, \quad (28)$$

see (24) and (27). Note that  $S_k$ , as  $W_k$  for the MCPW, can be scaled arbitrarily. Following the analysis in [23, Sec. 2.1], we finally obtain the half-space capacitance matrix *in vacuo* of the MCPW as:

$$\mathbf{C}_{\text{uh0}}^{\text{MCPS}} = -\epsilon_0 \mathbf{L}^{-1} \cdot \mathbf{F}^{-1} \cdot \mathbf{G}, \quad (29)$$

where  $\mathbf{L}^{-1} = [\mathbf{U}^{-1}]^T$ . Note that the ground reference can be easily moved from strip  $N + 1$  to another one by defining the so-called augmented,  $(N + 1) \times (N + 1)$  capacitance matrix  $\mathbf{C}'$ . Introducing the potential of strip  $V_{N+1}$ , straightforward circuit analysis yields for the elements of  $\mathbf{C}'$ :

$$\begin{aligned} C'_{i,N+1} &= -\sum_{j=1}^N C_{ij}, & C'_{N+1,j} &= -\sum_{i=1}^N C_{ij}, \\ C'_{N+1,N+1} &= \sum_{i=1}^N \sum_{j=1}^N C_{ij}. \end{aligned} \quad (30)$$

By cancelling column and row  $n$ , the capacitance matrix with the ground at strip  $n$  is obtained. The same approach can be used if a set of strips is grounded to minimize coupling and crosstalk, as in MCPS interconnects with shield lines [25].

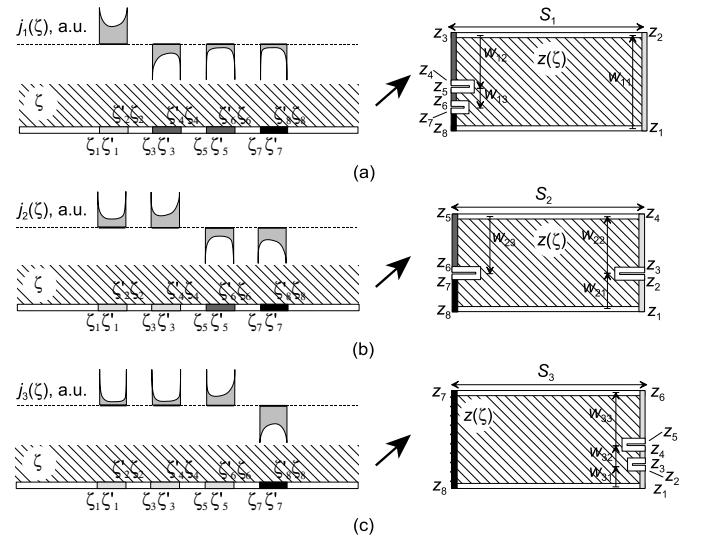


Fig. 5. Set of SC mappings (a), (b), and (c) for a three-conductor symmetric MCPS. Slots are drawn as white segments, the equipotential strips from 1-st to  $k$ -th strip are pale grey, all other zero-potential strips are dark grey and the ground plane (strip  $N + 1$ ) is black. White segments also denote magnetic walls. The right-hand side  $z$  planes are to scale, assuming  $S_k = S$ ,  $k = 1 \dots 3$ . The normalized static charge, i.e., the high-frequency surface current density distribution, is shown on the left side (above) for each mapping.



### III. EVALUATING THE SKIN-EFFECT CONDUCTOR LOSSES

For both the MCPW and the MCPS, the square-integrable normalized (dimensionless) surface current density distribution in the  $t$  plane is expressed, for the  $k$ -th mapping (see (19) and (1)), as:

$$j_k(t) = \frac{dz_k}{d\zeta} \left| \frac{d\zeta}{dt} \right| = \frac{\sum_{i=1}^N a_{ki} \zeta^{i-1}}{\left\{ \Re \right\} \prod_{i=1}^{2N+2} \sqrt{\zeta - \zeta_i}} \prod_{i=1}^{2N+2} \sqrt{\left| \frac{\zeta_i - \zeta}{\zeta'_i - \zeta} \right|} \quad (31)$$

taking into account that the current density in the  $k$ -th strip in the transformed  $z$  plane is uniform due to the parallel-plate geometry. The real ( $\Re$ ) and imaginary ( $\Im$ ) parts apply to the MCPW and MCPS case, respectively. The surface current density in the upper half-space,  $J_{uh}(t)$ , induced by an arbitrary excitation, can be represented as the superposition, with weights  $\hat{I}_k$  (unit A/m) of the  $j_k$  resulting from all linearly independent mappings:

$$J_{uh}(t) = \sum_{k=1}^N \hat{I}_k j_k(t). \quad (32)$$

The total current in the  $l$ -th line ( $l = 1 \dots N$ ,  $l = N + 1$  corresponds to the ground plane) is obtained from integration as:

$$\begin{aligned} I_l &= \oint \sum_{k=1}^N \hat{I}_k j_k(t) dt = 2 \int_l J_{uh}(t) dt = \\ &= 2 \sum_{k=1}^N \hat{I}_k \int_l \frac{dz_k}{d\zeta} \left| \frac{d\zeta}{dt} \right| dt = 2 \sum_{k=1}^N \hat{I}_k \int_l dz_k \end{aligned} \quad (33)$$

where the integral refers to the strip upper half and the factor 2 takes into account the strip lower half. We will now evaluate the line current and the dissipated power for the MCPW (Sec. III-A) and the MCPS (Sec. III-B) case.

#### A. MCPW conductor losses

For the MCPW, mapping  $k$  yields a total nonzero current in strip  $l = k$  only and in the ground planes. Therefore, using (20), (21) and (22) in (33), the total strip and ground planes currents in the  $k$ -th mapping can be expressed as:

$$I_l = -2\hat{I}_k W_k, \quad l = k, \quad I_l = 0, \quad l \neq k, \quad I_{N+1} = 2\hat{I}_k W_k. \quad (34)$$

Deriving  $\hat{I}_k$  and using (32), the surface current density resulting from the superposition of all mappings is:

$$J_{uh}(t) = - \sum_{k=1}^N \frac{I_k}{2W_k} j_k(t). \quad (35)$$

The total power dissipated *p.u.l.* on all lines and the ground plane can now be expressed as follows:

$$\begin{aligned} P_{diss} &= R_S \oint_{\text{ground} + \text{lines}} J^2(t) dt = \frac{1}{2} R_S \sum_{l,m=1}^N \frac{I_l}{W_l} \frac{I_m}{W_m} \times \\ &\times \sum_{n=1}^{N+1} \int_n j_l(t) j_m(t) dt \equiv \sum_{l,m=1}^N I_l R_{lm}^{\text{MCPW}} I_m. \end{aligned} \quad (36)$$

where  $R_S = 1/(\sigma\delta)$  is the surface resistance,  $\sigma$  being the metal conductivity and  $\delta$  the skin penetration depth. In (36) the integral on the  $n$ -th line (or on the ground plane for  $n = N + 1$ ) refers to the upper half space, and  $R_{lm}^{\text{MCPW}}$  is the *p.u.l.* resistance matrix element, that can be thus expressed as:

$$R_{lm}^{\text{MCPW}} = \sum_{n=1}^{N+1} R_{lm,n}^{\text{MCPW}} \quad (37)$$

where  $R_{lm,n}^{\text{MCPW}}$  derives from integration on strip  $n$ , or on the ground plane for  $n = N + 1$ . Taking into account the  $t \rightarrow \zeta$  and  $\zeta \rightarrow z_k$  mappings in (31) we have:

$$R_{lm,n}^{\text{MCPW}} = \frac{R_S}{2W_l W_m} \int_n \frac{dz_l}{d\zeta} \frac{dz_m}{d\zeta} \left| \frac{d\zeta}{dt} \right| d\zeta, \quad (38)$$

where the integral will be referred to as the *loss integral* of strip  $n$ . The present treatment generalizes the analysis in [14], [15], [18]; details of the evaluation of the loss integrals are omitted since the procedure closely follows [15]. The same result is obtained by integration of the edge-singular loss integrand of the zero-thickness line using the Lewin-Vainshtein (LV) high-frequency limit as the stopping distance [21]. The loss integral expressions can be extended down to the frequency range where  $\delta \approx \tau$  by replacing the LV limit  $\Delta_{LV} = \tau/(4\pi e^\pi)$  with the stopping distance  $\Delta(f)$ , i.e., by setting  $\tau/(4\pi) \rightarrow e^\pi \Delta$  [17] in (39), (40), (54) and (55), and by replacing  $R_S$  with the generalized resistance  $R_{sm}$  defined in [21, (8)]. In the high-frequency limit we obtain:

$$\begin{aligned} R_{hk,n}^{\text{MCPW}} &= \frac{R_S}{2W_h W_k} \left\{ \left[ \frac{\phi_{hk}(\bar{\zeta}_{2n})}{\xi(\bar{\zeta}_{2n})} - \frac{\phi_{hk}(\bar{\zeta}_{2n+1})}{\xi(\bar{\zeta}_{2n+1})} \right] \times \right. \\ &\times \left[ \pi + \ln \frac{4\pi}{\tau} (\bar{\zeta}_{2n+1} - \bar{\zeta}_{2n}) \right] + \\ &+ \sum_{l=1, l \neq 2n, 2n+1}^{2N+2} \frac{\phi_{hk}(\bar{\zeta}_l)}{\xi(\bar{\zeta}_l)} \ln \frac{\zeta'_{2n+1} - \bar{\zeta}_l}{\zeta'_{2n} - \bar{\zeta}_l} \left. \right\}, \quad n = 1 \dots N \end{aligned} \quad (39)$$

$$\begin{aligned} R_{hk,N+1}^{\text{MCPW}} &= \frac{R_S}{2W_h W_k} \left\{ \left[ \frac{\phi_{hk}(\bar{\zeta}_{2N+2})}{\xi(\bar{\zeta}_{2N+2})} - \frac{\phi_{hk}(\bar{\zeta}_1)}{\xi(\bar{\zeta}_1)} \right] \times \right. \\ &\times \left[ \pi + \ln \frac{4\pi}{\tau} (\bar{\zeta}_{2N+2} - \bar{\zeta}_1) \right] + \\ &+ \sum_{l=2}^{2N+1} \frac{\phi_{hk}(\bar{\zeta}_l)}{\xi(\bar{\zeta}_l)} \ln \frac{\bar{\zeta}_l - \zeta'_1}{\zeta'_{2N+2} - \bar{\zeta}_l} \left. \right\}, \end{aligned} \quad (40)$$

where:

$$\bar{\zeta}_l = \frac{\zeta_i + \zeta'_i}{2} \quad (41)$$

$$\xi(\bar{\zeta}_l) = \prod_{i=1, i \neq l}^{2N+2} (\bar{\zeta}_l - \bar{\zeta}_i) \quad (42)$$

$$\phi_{hk}(\bar{\zeta}_l) = \left( \sum_{i=1}^N a_{hi} \bar{\zeta}_l^{i-1} \right) \left( \sum_{j=1}^N a_{kj} \bar{\zeta}_l^{j-1} \right). \quad (43)$$

The resistance matrix elements can be obtained from (37).

### B. MCPS conductor losses

In the MCPS case the terms  $l = 1 \dots N$  in (33) correspond to lines, while  $l = N+1$  to the rightmost ground plane. Taking into account that integration of the MCPS  $k$ -th mapping yields:

$$\int_l \frac{dz_k}{d\zeta} d\zeta = \int_l dz_k = w_{kl} > 0, \quad l \leq k \quad (44)$$

$$\int_l \frac{dz_k}{d\zeta} d\zeta = \int_l dz_k = w_{kl} < 0, \quad l > k \quad (45)$$

$$\int_{N+1} \frac{dz_k}{d\zeta} d\zeta = \int_{N+1} dz_k = -\sum_{l=1}^N w_{kl}, \quad (46)$$

the line and ground plane currents can be expressed as:

$$I_k = 2 \sum_{l=1}^N w_{kl} \hat{I}_l, \quad k = 1 \dots N \quad (47)$$

$$I_{N+1} = -2 \sum_{k=1}^N \sum_{l=1}^N w_{kl} \hat{I}_l. \quad (48)$$

Equation (47) is a linear system with matrix  $2\mathbf{w}^T$  (28); define  $\mathbf{u} = (\mathbf{w}^T)^{-1}$ , with elements  $u_{kl}$ ; inverting (47) one has:

$$\hat{I}_k = \frac{1}{2} \sum_{l=1}^N u_{kl} I_l \quad (49)$$

and, from (32), the upper half-plane surface current density reads:

$$J_{uh}(t) = \sum_{k=1}^N \sum_{l=1}^N \frac{u_{kl} I_l}{2} j_k(t). \quad (50)$$

The total power dissipated on all lines and the ground plane can be expressed as a quadratic form of the strip total currents as follows:

$$\begin{aligned} P_{\text{diss}} &= R_S \oint_{\text{ground} + \text{lines}} J^2(t) dt = \\ &= 2R_S \sum_{l,m=1}^N I_l I_m \sum_{k,h=1}^N \frac{u_{kl}}{2} \frac{u_{hm}}{2} \oint_{\text{ground} + \text{lines}} j_k(t) j_h(t) dt = \\ &= \frac{1}{2} R_S \sum_{l,m=1}^N I_l I_m \sum_{k,h=1}^N u_{kl} u_{hm} \sum_{n=1}^{N+1} \int_n j_k(t) j_h(t) dt = \\ &\equiv \sum_{l,m=1}^N I_l R_{lm}^{\text{MCPS}} I_m, \end{aligned} \quad (51)$$

where the integral on the  $n$ -th line, or on the ground plane for  $n = N+1$ , refers to the upper half space. Thus the elements of the *p.u.l.* resistance matrix of the MCPS are expressed as in (37) with MCPW  $\rightarrow$  MCPS:

$$R_{lm}^{\text{MCPS}} = \sum_{n=1}^{N+1} R_{lm,n}^{\text{MCPS}}, \quad (52)$$

$R_{lm}^{\text{MCPS}}$  derives from integration on strip  $n$  or on the ground plane,  $n = N+1$ . Taking into account the  $t \rightarrow \zeta$  mapping and the  $\zeta \rightarrow z_k$  mappings we have:

$$\begin{aligned} R_{lm,n}^{\text{MCPS}} &= \frac{R_S}{2} \sum_{k,h=1}^N u_{kl} u_{hm} \int_n \frac{dz_k}{d\zeta} \frac{dz_h}{d\zeta} \left| \frac{d\zeta}{dt} \right| d\zeta \\ &\equiv \sum_{k,h=1}^N u_{kl} u_{hm} \hat{R}_{kh,n}^{\text{MCPS}}. \end{aligned} \quad (53)$$

Following an approach similar to the MCPW case we obtain:

$$\begin{aligned} \hat{R}_{kh,n}^{\text{MCPS}} &= \frac{R_S}{2} \left\{ \left[ \frac{\phi_{hk}(\bar{\zeta}_{2n})}{\xi(\bar{\zeta}_{2n})} - \frac{\phi_{hk}(\bar{\zeta}_{2n-1})}{\xi(\bar{\zeta}_{2n-1})} \right] \times \right. \\ &\quad \times \left[ \pi + \ln \frac{4\pi}{\tau} (\bar{\zeta}_{2n} - \bar{\zeta}_{2n-1}) \right] + \\ &\quad \left. - \sum_{l=1, l \neq 2n-1, 2n}^{2N+2} \frac{\phi_{hk}(\bar{\zeta}_l)}{\xi(\bar{\zeta}_l)} \ln \frac{\zeta'_{2n} - \bar{\zeta}_l}{\zeta'_{2n-1} - \bar{\zeta}_l} \right\} \end{aligned} \quad (54)$$

$$\begin{aligned} \hat{R}_{kh,N+1}^{\text{MCPS}} &= \frac{R_S}{2} \left\{ \left[ \frac{\phi_{hk}(\bar{\zeta}_{2N+2})}{\xi(\bar{\zeta}_{2N+2})} - \frac{\phi_{hk}(\bar{\zeta}_{2N+1})}{\xi(\bar{\zeta}_{2N+1})} \right] \times \right. \\ &\quad \times \left[ \pi + \ln \frac{4\pi}{\tau} (\bar{\zeta}_{2N+2} - \bar{\zeta}_{2N+1}) \right] + \\ &\quad \left. - \sum_{l=1}^{2N} \frac{\phi_{hk}(\bar{\zeta}_l)}{\xi(\bar{\zeta}_l)} \ln \frac{\zeta'_{2N+2} - \bar{\zeta}_l}{\zeta'_{2N+1} - \bar{\zeta}_l} \right\}, \end{aligned} \quad (55)$$

where  $\bar{\zeta}$ ,  $\xi$  and  $\phi$  are again defined in (41), (42) and (43), respectively. On defining the matrices  $\mathbf{R}_n^{\text{MCPS}} = [\hat{R}_{lm,n}^{\text{MCPS}}]$ ,  $\hat{\mathbf{R}}_n^{\text{MCPS}} = [\hat{R}_{lm,n}^{\text{MCPS}}]$ ,  $\mathbf{R}^{\text{MCPS}} = [\hat{R}_{lm}^{\text{MCPS}}] = \sum_n \mathbf{R}_n^{\text{MCPS}}$  and  $\hat{\mathbf{R}}^{\text{MCPS}} = [\hat{R}_{lm}^{\text{MCPS}}] = \sum_n \hat{\mathbf{R}}_n^{\text{MCPS}}$ , we have from (52) and (53) that the resistance matrix of the MCPS can be evaluated as:

$$\mathbf{R}^{\text{MCPS}} = \mathbf{u}^T \cdot \hat{\mathbf{R}}^{\text{MCPS}} \cdot \mathbf{u}, \quad (56)$$

where  $\mathbf{u} = (\mathbf{w}^T)^{-1}$ . Notice that the reference ground can be moved from strip  $N+1$  to an arbitrary strip  $n$  by transforming the resistance matrix  $\mathbf{R}^{\text{MCPS}}$  into the corresponding conductance matrix  $\mathbf{G}_m$  and deriving the augmented conductance matrix  $\mathbf{G}'_m$ , following the same rule as for the capacitance matrix, see (30). From  $\mathbf{G}'_m$  the conductance matrix with ground at strip  $n$  is recovered by canceling row and column  $n$ ; inversion finally yields the desired  $\mathbf{R}^{\text{MCPS}}$  with ground at strip  $n$ . The same approach holds for a MCPS with a set of grounded shield lines.

### IV. CHARACTERISTIC *p.u.l.* PARAMETERS, MODAL IMPEDANCES AND COMPLEX PROPAGATION CONSTANTS

We refer to a MCL on an infinitely thick dielectric substrate with relative permittivity  $\epsilon_r$  and conductivity  $\sigma_{\text{sub}}$ . Given the *in vacuo* capacitance matrix of the upper half space  $\mathbf{C}_{\text{uh0}}$  we have  $\mathbf{C} \approx (1 + \epsilon_r) \mathbf{C}_{\text{uh0}}$  for the capacitance matrix,  $\mathbf{L} = (2\mathbf{C}_{\text{uh0}})^{-1} / c_0^2 + \mathbf{R}(\omega) / \omega$  for the inductance matrix accounting for the skin-effect internal inductance, and  $\mathbf{G} \approx (\sigma_{\text{sub}} / \epsilon_0) \mathbf{C}_{\text{uh0}}$  for the conductance matrix associated to parallel substrate losses, where  $c_0$  is the velocity of light *in vacuo*. Notice that the assumptions  $\mathbf{C} = (1 + \epsilon_r) \mathbf{C}_{\text{uh0}}$  and

$\mathbf{G} = (\sigma_{\text{sub}}/\epsilon_0)\mathbf{C}_{\text{uh0}}$  only approximately hold for very thick lines, where the dielectric does not exactly fill one half space; thus the approximation signs. From the above matrices and  $\mathbf{R}$ , the *p.u.l.* impedance  $\mathbf{Z}$  and admittance  $\mathbf{Y}$  matrices can be evaluated as  $\mathbf{Z} = \mathbf{R} + j\omega\mathbf{L}$  and  $\mathbf{Y} = \mathbf{G} + j\omega\mathbf{C}$ . The modal complex propagation constants can be finally derived as the square roots of the eigenvalues of the product  $\mathbf{Z}\mathbf{Y}$ . The modal characteristic impedances according to the so-called power-current (PI), voltage-current (VI) and power-voltage (PV) definitions can be finally recovered through the eigenvector matrices of  $\mathbf{Z}\mathbf{Y}$  and  $\mathbf{Y}\mathbf{Z}$  [26].

## V. EXAMPLES

A few examples are discussed to test the consistency of the present approach with previously published quasi-static formulae and its accuracy vs. quasi-static and full-wave EM formulations. We will also use as a reference solution the numerical SC solver discussed in [27], [28] and used in [29] to evaluate the impedance and skin-effect losses of CPWs with arbitrarily shaped electrodes. In the examples shown the imaginary part of the characteristic impedance is negligible vs. the real part, simply denoted as “characteristic impedance”. In

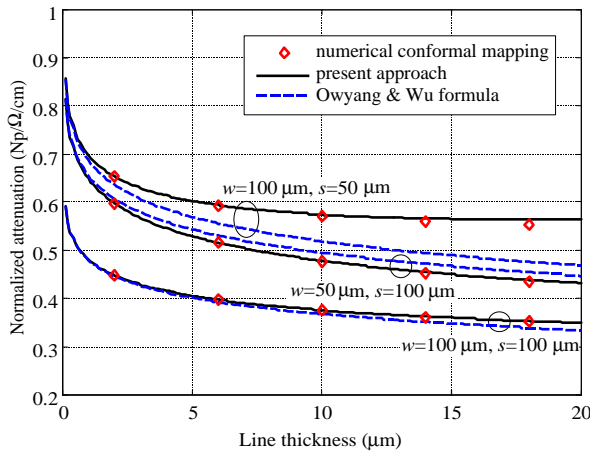


Fig. 6. Conductor normalized attenuation  $\alpha/R_s$  of a symmetric CPW ( $N = 1$ ) *in vacuo* as a function of line thickness with different values of the line width  $w$  and slot width  $s$ : numerical conformal mapping (diamonds) from [29]; present approach (black solid lines), formulae from [14] (blue dashed lines).

all computations shown the number of integration samples in the quadrature formulae [23, Sec. 3] is 20. Fig. 6 compares the normalized attenuation of a symmetric CPW *in vacuo* (MCPW with  $N = 1$ ) from the Owyang and Wu formula [14] with the present approach and the exact numerical CM solution from [29]. The present solution is in excellent agreement with the numerical CM also for line thickness as large as 40% of the strip or slot width, and provides a better approximation than the formulae in [14]. Fig. 7 compares the characteristic impedance of the same symmetric CPW *in vacuo* evaluated in the present approach and as in [29]; the agreement is again very good also for line thickness as large as 40% of the strip or slot width. Notice that in the approach of [14] the thick strip correction of the impedance is not considered.

Fig. 8 compares, for the attenuation of a CPS (MCPS with  $N = 1$ ), the analytical expressions in [15] with the present

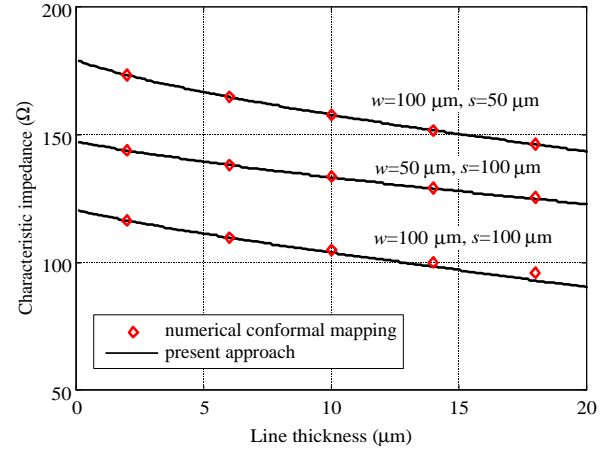


Fig. 7. Characteristic impedance of a symmetric CPW ( $N = 1$ ) *in vacuo* as a function of line thickness with different values of the line width  $w$  and slot width  $s$ : numerical conformal mapping (diamonds) from [29]; present approach (black solid lines).

approach and the exact numerical CM solution from [29]. As in the following examples, the frequency is  $f = 10$  GHz and the metal conductivity  $\sigma = 4.1 \times 10^7$  S/m. The present solution virtually coincides with the numerical CM and provides a better approximation than the formulae in [18], above all for low line spacing, as expected.

Comparisons concerning the modal attenuations and characteristic impedances, respectively, between the present approach and a full-wave and quasi-static FEM solution are presented in Fig. 9 and Fig. 10 for a five-conductor MCPW *in vacuo*. The present closed-form approach clearly yields an accurate estimate of both the attenuation and the modal impedances. Notice that the skin penetration depth at the operating frequency is  $\delta = 786$  nm; as well known the skin-effect approximation is in this case expected to be increasingly inaccurate for strip thickness  $\tau < n\delta$  with  $n \approx 4$ .

To the authors' best knowledge, no experimental data on the attenuation of multiconductor coplanar lines are available; however, an indirect comparison can be made from the data on the attenuation of finite-ground coplanar waveguides on a lossy Si substrate reported in [30]. Fig. 11 shows a comparison between the measured and simulated total attenuation as a function of frequency for two sets of lines, with strip and slot widths of 25 and 50  $\mu\text{m}$ , respectively, and varying finite ground widths (only the extreme values are simulated). The substrate losses were taken into account, and a satisfactory fit with measurements was obtained with an average conductivity of the composite metallization  $\sigma = 3 \times 10^7$  S/cm. The accuracy of the simulation degrades at lower frequencies where the strip thickness becomes comparable to the skin penetration depth. The parameters of the finite-ground CPW were obtained from those of a MCPS with two conductors plus ground, by grounding the leftmost strip.

Fig. 12 and Fig. 13 compare the attenuation and effective refractive index of a five-conductor (plus ground) MCPS *in vacuo* with the results of quasi-static FEM as a function of frequency. Notice that the effective refractive index variation vs. the *in vacuo* value, entirely related to conductor losses,



is accurately reproduced by the analytical model. The modal patterns shown in the figure insets are qualitative only, due to the asymmetry of the structure.

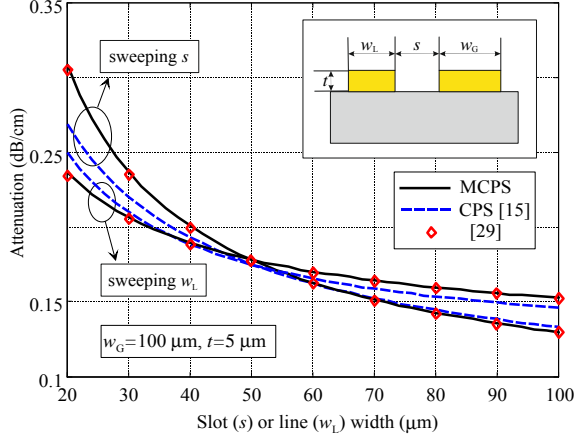


Fig. 8. Conductor attenuation of an asymmetric CPS ( $N = 1$ ) *in vacuo* as a function of line spacing  $s$  (with  $w_L = 50 \mu\text{m}$ ) or width  $w_L$  (with  $s = 50 \mu\text{m}$ ): present approach (black solid lines), formulae from [15] (blue dashed lines), numerical conformal mapping (diamonds) from [29]. The ground width is  $w_G = 100 \mu\text{m}$  and the conductor thickness is  $\tau = 5 \mu\text{m}$ .

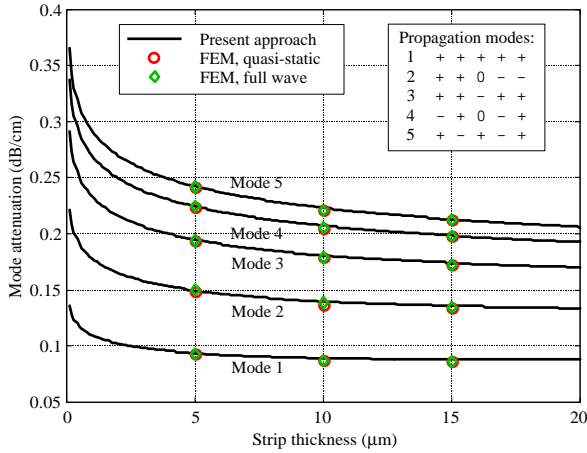


Fig. 9. Modal *in vacuo* conductor attenuations of a uniform symmetric five-conductor MCPW as a function of the line thickness: comparison between the present approach (black solid lines), quasi-static FEM (circles) [6] and full-wave FEM (diamonds) [5]. The line and slot widths are  $50 \mu\text{m}$ .

## VI. CONCLUSIONS

We have presented computationally efficient, accurate closed-form expressions for the conductor losses and the modal impedances of thick multiconductor coplanar lines. With respect to already available expressions for single and coupled lines, the present approach provides an estimate of the line characteristic parameters that is accurate even for line thicknesses of the order of 40% of the minimum slot or strip width. The results compare favorably with numerical CM implementations and with quasi-static and full-wave FEM simulations.

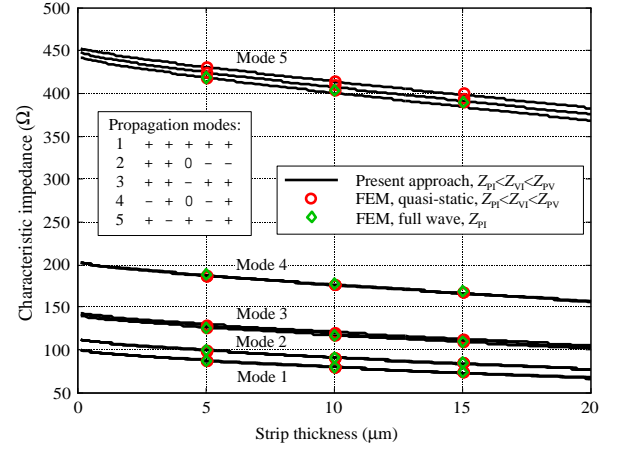


Fig. 10. Modal *in vacuo* characteristic impedances of a uniform symmetric five-conductor MCPW as a function of the line thickness: comparison between the present approach (black solid lines), quasi-static FEM (circles) [6] and full-wave FEM (diamonds) [5]. The line and slot widths are  $50 \mu\text{m}$ .

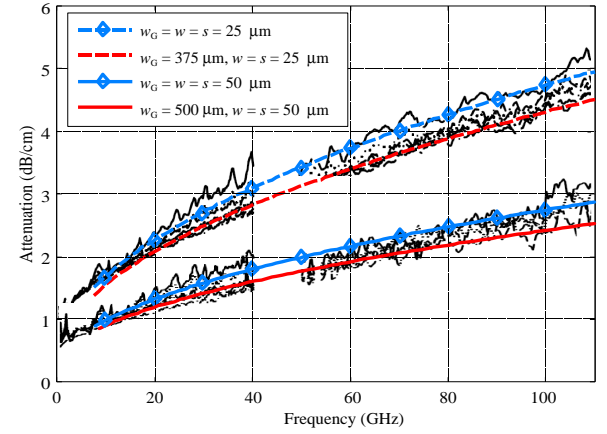


Fig. 11. Attenuation of a finite-ground CPW as a function of frequency for different values of the strip, slot and finite-extent ground plane width. The metal thickness is  $3 \mu\text{m}$ , the substrate is Si with resistivity  $2500 \Omega\cdot\text{cm}$  and  $\epsilon_r = 11.8$ . The measured curves from [30, Fig.3 (a), (b)] are for ground widths  $w_G$  between the two extremes considered in the simulation, namely for  $w_G = 25, 37, 50, 75, 125, 250, 375 \mu\text{m}$  (upper set, simulations with blue and red dashed lines), and  $w_G = 50, 75, 100, 150, 250, 500 \mu\text{m}$  (lower set, simulations with blue and red continuous lines). The measured and simulated attenuation decreases with increasing  $w_G$ .

## APPENDIX

### A. Strip side, strip and slot width corrections due to finite conductor thickness

The  $t \rightarrow \zeta$  transformation (1) cannot be inverted explicitly; however, if  $\tau \ll w, s$ , we can approximately invert the transformation for each strip side, strip top and each slot, accounting for the effect of nearby strips and slots.

Let us consider first the correction  $\Delta\zeta$  related to the thick conductor (strip or ground plane) side. Consider first the MCPW case; we have ( $i = 1 \dots N + 1$ ):

$$\begin{aligned} \int_{t_{2i-1}}^{t'_{2i-1}} dt &= j \frac{\tau}{2} = \int_{\zeta'_{2i-1}}^{\zeta_{2i-1}} \frac{dt}{d\zeta} d\zeta = \\ &= \int_{\zeta'_{2i-1}}^{\zeta_{2i-1}} \prod_{j=1}^{2N+2} \sqrt{\frac{\zeta'_j - \zeta}{\zeta_j - \zeta}} d\zeta \end{aligned} \quad (57)$$

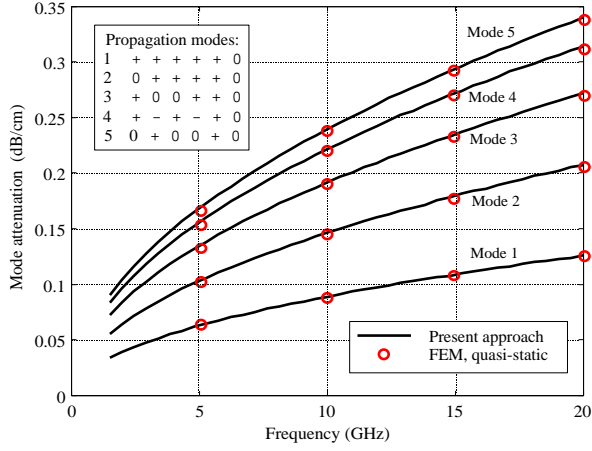


Fig. 12. Modal *in vacuo* conductor attenuations of a uniform five-conductor (plus ground) MCPW as a function of frequency: comparison between the present approach (black solid lines) and quasi-static FEM (circles) [6]. The line, slot and ground plane widths are  $50 \mu\text{m}$ . The conductor thickness is  $\tau = 5 \mu\text{m}$ . The metal conductivity is  $\sigma = 4.1 \times 10^7 \text{ S/m}$ .

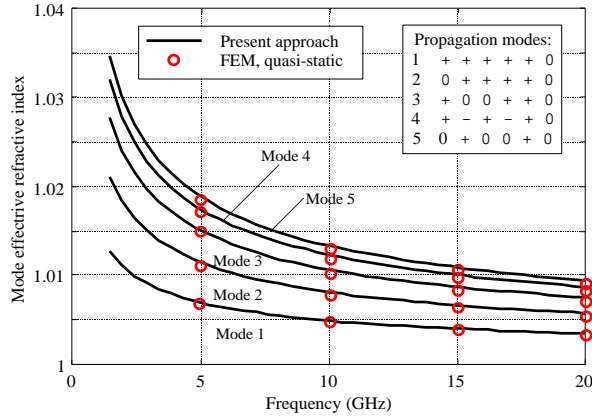


Fig. 13. Modal *in vacuo* effective refractive index of the five-conductor (plus ground) MCPW (see Fig. 12) as a function of frequency: comparison between the present approach (black solid lines) and quasi-static FEM (circles) [6].

$$\begin{aligned}
 &= \int_{\zeta'_{2i-1}}^{\zeta_{2i-1}} \prod_{j=1}^{2i-2} \sqrt{\frac{\zeta'_j - \zeta}{\zeta_j - \zeta}} \sqrt{\frac{\zeta - \zeta'_{2i-1}}{\zeta_{2i-1} - \zeta}} \prod_{j=2i}^{2N+2} \sqrt{\frac{\zeta - \zeta'_j}{\zeta_j - \zeta}} d\zeta \approx \\
 &\approx j \int_{\zeta'_{2i-1}}^{\zeta_{2i-1}} \sqrt{\frac{\zeta - \zeta'_{2i-1}}{\zeta_{2i-1} - \zeta}} d\zeta = j \frac{\pi}{2} (\zeta_{2i-1} - \zeta'_{2i-1}) = j \frac{\pi}{2} \Delta\zeta
 \end{aligned} \quad (58)$$

i.e.:

$$\zeta_{2i-1} - \zeta'_{2i-1} \approx \Delta\zeta = \frac{\tau}{\pi} \quad (59)$$

because:

$$\prod_{i=1, j \neq 2i}^{2N+2} \sqrt{\frac{\zeta'_j - \zeta}{\zeta_j - \zeta}} \approx 1, \quad \zeta_{2i} < \zeta < \zeta'_{2i}. \quad (60)$$

Similar results are obtained for the MCPW strip sides of even index and for the MCPW. It follows that each strip edge (including the ground planes) should be extended in plane  $\zeta$

by an amount that, in the first approximation, does not depend on the strip or ground plane width:

$$\begin{aligned} \Delta\zeta &= \zeta'_{2i} - \zeta_{2i} = \zeta_{2i-1} - \zeta'_{2i-1} = \\ &\approx \frac{\tau}{\pi}, \quad i = 1 \dots N+1 \text{ (MCPW)} \end{aligned} \quad (61)$$

$$\begin{aligned} \Delta\zeta &= \zeta'_{2i-1} - \zeta_{2i-1} = \zeta_{2i} - \zeta'_{2i} = \\ &\approx \frac{\tau}{\pi}, \quad i = 1 \dots N+1 \text{ (MCPS)}. \end{aligned} \quad (62)$$

Let us consider integrating transformation (1) on the strip tops. For simplicity, let us confine the detailed treatment to the MCPW strips and slots. We have:

$$\begin{aligned} t'_{2j+1} - t'_{2j} &= w_j = \\ &= \int_{\zeta'_{2j}}^{\zeta'_{2j+1}} \frac{dt}{d\zeta} d\zeta \quad i = 1 \dots N \end{aligned} \quad (63)$$

$$t_{2j} - t_{2j-1} = s_j = \int_{\zeta_{2j-1}}^{\zeta_{2j}} \frac{dt}{d\zeta} d\zeta \quad i = 1 \dots N+1. \quad (64)$$

The strip integral (63) can be approximated as follows:

$$\begin{aligned}
 t'_{2j+1} - t'_{2j} &= w_j = \\
 &= \int_{\zeta'_{2j}}^{\zeta'_{2j+1}} \prod_{i=1}^{2j-1} \sqrt{\frac{\zeta - \zeta'_i}{\zeta_i - \zeta}} \prod_{i=2j+2}^{2N+2} \sqrt{\frac{\zeta'_i - \zeta}{\zeta_i - \zeta}} \times \\
 &\times \left( \sqrt{\frac{\zeta - \zeta'_{2j}}{\zeta_i - \zeta_{2j}}} \sqrt{\frac{\zeta'_{2j+1} - \zeta}{\zeta_{2j+1} - \zeta}} \right) d\zeta \approx \\
 &\approx \prod_{i=1}^{2j-1} \left( 1 + \frac{(-1)^{i+1} \frac{\Delta\zeta}{2}}{\langle \zeta \rangle_j - \zeta_i} \right) \prod_{i=2j+2}^{2N+2} \left( 1 + \frac{(-1)^i \frac{\Delta\zeta}{2}}{\zeta_i - \langle \zeta \rangle_j} \right) \times \\
 &\times \int_{\zeta'_{2j}}^{\zeta'_{2j+1}} \sqrt{\frac{\zeta - \zeta'_{2j}}{\zeta_i - \zeta_{2j}}} \sqrt{\frac{\zeta'_{2j+1} - \zeta}{\zeta_{2j+1} - \zeta}} d\zeta \approx \\
 &\approx \left( 1 + \sum_{i=1}^{2j-1} \frac{(-1)^{i+1} \frac{\Delta\zeta}{2}}{\langle t \rangle_{\text{Strip } j} - t_i} + \sum_{i=2j+2}^{2N+2} \frac{(-1)^i \frac{\Delta\zeta}{2}}{t_i - \langle t \rangle_{\text{Strip } j}} \right) \times \\
 &\times \int_{\zeta'_{2j}}^{\zeta'_{2j+1}} \sqrt{\frac{\zeta - \zeta'_{2j}}{\zeta_i - \zeta_{2j}}} \sqrt{\frac{\zeta'_{2j+1} - \zeta}{\zeta_{2j+1} - \zeta}} d\zeta
 \end{aligned} \quad (66)$$

where  $\langle \zeta \rangle_j$  is the average coordinate of strip  $j$  in  $\zeta$  plane, that is approximated, to make the expression explicit, as  $\langle \zeta \rangle_j \approx \langle t \rangle_{\text{Strip } j}^{\text{MCPW}}$ , where:

$$\langle t \rangle_{\text{Strip } j}^{\text{MCPW}} = \frac{t_{2j+1} + t_{2j}}{2}. \quad (67)$$

The integral in (66) can be solved exactly in terms of complete elliptic integrals of the first and second kind [31, p. 308, (10)] and further approximated through the formulae in [31, Sec. 8.113, (3) and Sec. 8.114, (3)] under the assumption  $\tau \ll w_j$ , leading to the result:

$$\begin{aligned}
 &\int_{\zeta'_{2j}}^{\zeta'_{2j+1}} \sqrt{\frac{\zeta - \zeta'_{2j}}{\zeta_i - \zeta_{2j}}} \sqrt{\frac{\zeta'_{2j+1} - \zeta}{\zeta_{2j+1} - \zeta}} d\zeta \approx \\
 &\approx w_j + \Delta w_j - \Delta\zeta \left( \log \frac{4w_j}{\Delta\zeta} - 1 \right).
 \end{aligned} \quad (68)$$

Combining (68) with (66) and under the assumption of small  $\Delta\zeta$  we finally obtain (15).

Similarly, the slot integral (64) can be approximated as follows:

$$\begin{aligned}
 t_{2j} - t_{2j-1} &= s_j = \\
 &= \int_{\zeta_{2j-1}}^{\zeta_{2j}} \frac{dt}{d\zeta} d\zeta = \int_{\zeta_{2j-1}}^{\zeta_{2j}} \prod_{i=1}^{2j-2} \sqrt{\frac{\zeta - \zeta'_i}{\zeta - \zeta_i}} \times \\
 &\times \left( \sqrt{\frac{\zeta - \zeta'_{2j-1}}{\zeta - \zeta_{2j-1}}} \sqrt{\frac{\zeta'_{2j} - \zeta}{\zeta_{2j} - \zeta}} \right) \prod_{i=2j+1}^{2N+2} \sqrt{\frac{\zeta'_i - \zeta}{\zeta_i - \zeta}} d\zeta = \\
 &\approx \prod_{i=1}^{2j-2} \left( 1 + \frac{1}{2} \frac{(-1)^{i+1} \Delta\zeta}{\langle \zeta \rangle_j - \zeta_i} \right) \prod_{i=2j+1}^{2N+2} \left( 1 + \frac{1}{2} \frac{(-1)^i \Delta\zeta}{\zeta_i - \langle \zeta \rangle_j} \right) \times \\
 &\times \int_{\zeta_{2j-1}}^{\zeta_{2j}} \sqrt{\frac{\zeta - \zeta'_{2j-1}}{\zeta - \zeta_{2j-1}}} \sqrt{\frac{\zeta'_{2j} - \zeta}{\zeta_{2j} - \zeta}} d\zeta \approx \\
 &\approx \prod_{i=1}^{2j-2} \left( 1 + \frac{(-1)^{i+1} \frac{\Delta\zeta}{2}}{\langle t \rangle_{\text{Slot } j}^{\text{MCPW}} - t_i} \right) \prod_{i=2j+1}^{2N+2} \left( 1 + \frac{(-1)^i \frac{\Delta\zeta}{2}}{t_i - \langle t \rangle_{\text{Slot } j}^{\text{MCPW}}} \right) \times \\
 &\times \int_{\zeta_{2j-1}}^{\zeta_{2j}} \sqrt{\frac{\zeta - \zeta'_{2j-1}}{\zeta - \zeta_{2j-1}}} \sqrt{\frac{\zeta'_{2j} - \zeta}{\zeta_{2j} - \zeta}} d\zeta \approx \\
 &\approx \left( 1 + \sum_{i=1}^{2j-2} \frac{(-1)^{i+1} \frac{\Delta\zeta}{2}}{\langle t \rangle_{\text{Slot } j}^{\text{MCPW}} - t_i} + \sum_{i=2j+1}^{2N+2} \frac{(-1)^i \frac{\Delta\zeta}{2}}{t_i - \langle t \rangle_{\text{Slot } j}^{\text{MCPW}}} \right) \times \\
 &\times \int_{\zeta_{2j-1}}^{\zeta_{2j}} \sqrt{\frac{\zeta - \zeta'_{2j-1}}{\zeta - \zeta_{2j-1}}} \sqrt{\frac{\zeta'_{2j} - \zeta}{\zeta_{2j} - \zeta}} d\zeta \quad (69)
 \end{aligned}$$

where:

$$\langle t \rangle_{\text{Slot } j}^{\text{MCPW}} = \frac{t_{2j} + t_{2j-1}}{2}. \quad (70)$$

The integral in (69) can be solved exactly in terms of complete elliptic integrals of the second kind [31, p. 308, (14)] and further approximated through the formulae in [31, Sec. 8.114, (3)] assuming  $\tau \ll w_j$ ; this leads to the result:

$$\begin{aligned}
 &\int_{\zeta_{2j-1}}^{\zeta_{2j}} \sqrt{\frac{\zeta - \zeta'_{2j-1}}{\zeta - \zeta_{2j-1}}} \sqrt{\frac{\zeta'_{2j} - \zeta}{\zeta_{2j} - \zeta}} d\zeta \approx \\
 &\approx s_j - \Delta s_j + \Delta\zeta \left( \log \frac{4s_j}{\Delta\zeta} + 1 \right). \quad (71)
 \end{aligned}$$

Combining (71) with (69) and in the assumption of small  $\Delta\zeta$  we obtain (16).

The treatment of the MCPS strip and slot corrections is similar, leading to the results reported in (17) and (18). Notice that no strip or slot corrections are applied when the strip or slot has infinite extent.

## REFERENCES

- [1] R. Simons, *Coplanar Waveguide Circuits, Components, and Systems*. Hoboken, NJ: John Wiley & Sons, 2001.
- [2] I. Wolff, *Coplanar Microwave Integrated Circuits*. Hoboken, NJ: John Wiley & Sons, 2006.
- [3] C. P. Wen, "Coplanar-waveguide directional couplers," *IEEE Trans. Microwave Theory Techn.*, vol. MTT-18, no. 6, pp. 318–322, Jun. 1970.
- [4] J. Davis and J. D. Meindl, Eds., *Interconnect Technology and Design for Gigascale Integration*. Springer Science+Business Media, 2003.
- [5] F. Bertazzi, O. A. Peverini, M. Goano, G. Ghione, R. Orta, and R. Tascone, "A fast reduced-order model for the full-wave FEM analysis of lossy inhomogeneous anisotropic waveguides," *IEEE Trans. Microwave Theory Techn.*, vol. MTT-50, no. 9, pp. 2108–2114, Sep. 2002.
- [6] F. Bertazzi, G. Ghione, and M. Goano, "Efficient quasi-TEM frequency-dependent analysis of lossy multiconductor lines through a fast reduced-order FEM model," *IEEE Trans. Microwave Theory Techn.*, vol. MTT-51, no. 9, pp. 2029–2035, Sep. 2003.
- [7] R. Harrington, "Losses on multiconductor transmission lines in multilayered dielectric media," *IEEE Trans. Microwave Theory Techn.*, vol. 32, no. 7, pp. 705–710, Jul. 1984.
- [8] J. Aguilera, R. Marqués, and M. Horno, "Improved quasi-static spectral domain analysis of microstrip lines on high-conductivity insulator-semiconductor substrates," *IEEE Microwave Guided Wave Lett.*, vol. 9, no. 2, pp. 57–59, Feb. 1999.
- [9] F. Olyslager, D. De Zutter, and K. Blomme, "Rigorous analysis of the propagation characteristics of general lossless and lossy multiconductor transmission lines in multilayered media," *IEEE Trans. Microwave Theory Techn.*, vol. MTT-41, no. 1, pp. 79–88, Jan. 1993.
- [10] E. Soliman, G. Vandenbosch, E. Beyne, and R. Mertens, "Full-wave analysis of multiconductor multislot planar guiding structures in layered media," *IEEE Trans. Microwave Theory Techn.*, vol. 51, no. 3, pp. 874–886, Mar. 2003.
- [11] S. V. Yuferev and N. Ida, *Surface Impedance Boundary Conditions*. CRC Press, 2010.
- [12] W. Thomson, "On alternate currents in parallel conductors of homogeneous or heterogeneous substance," in *Mathematical and Physical Papers. Lord Kelvin, J. Larmor, Ed.* Cambridge University Press, 2011, vol. V, pp. 489–495.
- [13] J. D. Cockcroft, "Skin effect in rectangular conductors at high frequencies," *Proc. R. Soc. Lond. A, Math. Phys. Sci.*, vol. 122, no. A 790, p. 533542, February 1929.
- [14] G. H. Owyang and T. T. Wu, "The approximate parameters of slot lines and their complement," *IRE Trans. Antennas Propagation*, vol. 6, no. 1, pp. 49–55, Jan. 1958.
- [15] G. Ghione, "A CAD-oriented analytical model for the losses of general asymmetric coplanar lines in hybrid and monolithic MICs," *IEEE Trans. Microwave Theory Techn.*, vol. MTT-41, no. 9, pp. 1499–1510, Sep. 1993.
- [16] G. Ghione and M. Goano, "The influence of ground plane width on the ohmic losses of coplanar waveguides with finite lateral ground planes," *IEEE Trans. Microwave Theory Techn.*, vol. MTT-45, no. 9, pp. 1640–1642, Sep. 1997.
- [17] M. Duyar, V. Akan, E. Yazgan, and M. Bayrak, "Analytical attenuation calculation of asymmetrical coplanar waveguide with finite-extent ground planes for coplanar waveguide mode," *Microwave and Optical Technology Letters*, vol. 49, no. 9, pp. 2082–2087, 2007.
- [18] G. Ghione and M. Goano, "A closed-form CAD-oriented model for the high-frequency conductor attenuation of symmetrical coupled coplanar waveguides," *IEEE Trans. Microwave Theory Techn.*, vol. MTT-45, no. 7, pp. 1065–1070, Jul. 1997.
- [19] K. C. Gupta, R. Garg, I. Bahl, and P. Bhartia, *Microstrip Lines and Slotlines*, 2nd ed. Norwood, MA: Artech House, 1996.
- [20] H. A. Wheeler, "Formulas for the skin effect," *Proc. IRE*, vol. 30, no. 8, pp. 412–424, Sep. 1942.
- [21] C. L. Holloway and E. F. Kuester, "A quasi-closed form expression for the conductor loss of CPW lines, with an investigation of edge shape effects," *IEEE Trans. Microwave Theory Techn.*, vol. MTT-43, no. 12, pp. 2695–2701, Dec. 1995.
- [22] L. J. P. Linnér, "A method for the computation of the characteristic immittance matrix of multiconductor striplines with arbitrary widths," *IEEE Trans. Microwave Theory Techn.*, vol. MTT-22, no. 11, pp. 930–937, Nov. 1974.
- [23] G. Ghione, "An efficient, CAD-oriented model for the characteristic parameters of multiconductor buses in high-speed digital GaAs ICs," *Analog Integrated Circuits Signal Processing*, vol. 5, no. 1, pp. 67–75, Jan. 1994, also in M. S. Nakhla, Q. J. Zhang, *Modeling and Simulation of High Speed VLSI Interconnects*, pp. 67–74, Springer, 1994.
- [24] G. Ghione, M. Goano, and C. U. Naldi, "A CAD-oriented model for the ohmic losses of multiconductor coplanar lines in hybrid and monolithic MIC's," in *Gallium Arsenide Applications Symposium (GAAS 96)*, Paris, Jun. 1996, p. 8A2.
- [25] M. A. Elgamel and M. A. Bayoumi, Eds., *Interconnect Noise Optimization in Nanometer Technologies*. Springer, 2006.
- [26] C. R. Paul, *Analysis of Multiconductor Transmission Lines, 2nd Edition*. Wiley-IEEE Press, November 2007.

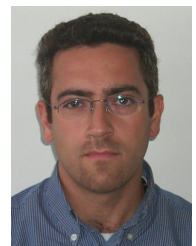
- [27] T. A. Driscoll, "Algorithm 756: A MATLAB toolbox for Schwarz-Christoffel mapping," *ACM Trans. Math. Software*, vol. 22, no. 2, pp. 168–186, Jun. 1996.
- [28] T. A. Driscoll and L. N. Trefethen, *Schwarz-Christoffel Mapping*. Cambridge, U.K.: Cambridge University Press, 2002.
- [29] M. Goano, F. Bertazzi, P. Caravelli, G. Ghione, and T. A. Driscoll, "A general conformal-mapping approach to the optimum electrode design of coplanar waveguides with arbitrary cross section," *IEEE Trans. Microwave Theory Techn.*, vol. MTT-49, no. 9, pp. 1573–1580, Sep. 2001.
- [30] G. E. Ponchak, L. P. B. Katehi, and E. M. Tentzeris, "Finite ground coplanar (FGC) waveguide: Its characteristics and advantages for use in RF and wireless communication circuits," in *3rd International Wireless Communications Conference (WCC 98) Digest*, Nov. 1998, pp. 75–83.
- [31] I. S. Gradshteyn and I. M. Ryzhik, *Tables of Integrals, Series, and Products*, 5th ed., A. Jeffrey, Ed. San Diego, CA: Academic Press, 1994.



**Marco Pirola** (M'97) was born in Velezzo Lomellina, Italy, in 1963. He received the Laurea degree in electronic engineering and the Ph.D. degree from Politecnico di Torino, Italy, in 1987 and 1992 respectively. In 1992 and 1994, he was a Visiting Researcher at the Hewlett Packard Microwave Technology Division, Santa Rosa, CA. Since 1992, he has been with the Electronic Department of Politecnico di Torino, first as researcher and, since 2000, as associate professor, where his research concerns the simulation, modeling and measurements of microwave devices and systems.



**Francesco Bertazzi** received the Laurea and Ph.D. degrees in Electronics Engineering from Politecnico di Torino in 2000 and 2003, respectively. From 2004 to 2008, he was Visiting Scholar at Boston University. Since 2008 he is Professor in the Dipartimento di Elettronica e Telecomunicazioni, Politecnico di Torino. His research activity is focused on the modeling of electronic transport in nanodevices by means of full-band Monte Carlo and nonequilibrium Greens function techniques. His interests also include recombination mechanisms in light emitters, electromagnetic propagation and noise in microwave devices.



both linear and nonlinear and power amplifier design. Dr. Camarchia was the recipient of the 2002 Young Graduated Research Fellowship presented by the Gallium Arsenide application Symposium (GAAS) Association.

**Vittorio Camarchia** (S'01-M'04-SM'14) received the Laurea degree in electronic engineering and the Ph.D. degree in electronic and communications engineering from the Politecnico di Torino, Turin, Italy, in 2000 and 2003, respectively. In 2001, 2002 and 2003 he was a Visiting researcher with the ECE Department, Boston University, Boston, MA, USA. He is currently an Associate Professor at the Electronics and Telecommunication Department of Politecnico di Torino. His research is focused on RF device modeling, simulation, and characterization,



of widegap semiconductor devices and materials. He has also done research in the field of microwave electronics, with contributions in the modeling of passive elements, in particular coplanar components, and in the design of power MMICs. Prof. Ghione was actively engaged since 1985 in research on optoelectronic devices, with application to the modeling and design of near and far-IR photodetectors, electrooptic and electroabsorption modulators, and GAN-based LEDs. Prof. Ghione has authored or co-authored more than 300 research papers on the above subjects and five books. He has been a member of the QPC subcommittee of IEDM in 1997-1998 and in 2006-2007 and Chair in 2008; in 2009-2010 he was the EU Arrangement Co-Chair of IEDM. From 2010 to 2015 he has been chair of the EDS Committee on Compound Semiconductor Devices and Circuits. From 2007 to 2015 he was the Head of the Department of Electronics and Telecommunications of Politecnico di Torino. Prof. Ghione is the Editor in Chief of the IEEE Transaction on Electron Devices for the period 2016-2018.

**Giovanni Ghione** (M'87-SM'94-F'07) graduated cum laude in Electronic Engineering from Politecnico di Torino, Torino, Italy in 1981. He is Full Professor in Electronics with Politecnico di Torino. His research activity has been mainly concerned with high-frequency electronics and optoelectronics. He has contributed to the physics-based modelling of compound semiconductor devices, with particular interest in the numerical noise modeling in the small- and large-signal regimes, in the thermal modeling of devices and integrated circuits, and in the modeling



MA, in 2000 and 2001. Since 1996, he has been with the Dipartimento di Elettronica e Telecomunicazioni, Politecnico di Torino, Turin, first as a Research Assistant and since 2005 as an Associate Professor. His present research activity is focused on the simulation of (opto)electronic devices based on narrow- and wide-bandgap semiconductor materials.

**Michele Goano** (M'98) received the Laurea and Ph.D. degrees in electronic engineering from Politecnico di Torino, Turin, Italy, in 1989 and 1993, respectively. He was a post-doctoral fellow with the Département de Génie Physique, École Polytechnique de Montréal, Montréal, QC, Canada, in 1994 and 1995. He was a visiting scholar with the School of Electrical and Computer Engineering, Georgia Institute of Technology, Atlanta, in 1998 and 1999, and with the Department of Electrical and Computer Engineering, Boston University, Boston,